Numerical Modeling of Electrostatic Discharge Generators

Kai Wang, *Member, IEEE*, David Pommerenke, Ramachandran Chundru, Tom Van Doren, *Fellow, IEEE*, James L. Drewniak, *Senior Member, IEEE*, and Ashwin Shashindranath

Abstract—The discharge current and the transient fields of an electrostatic discharge (ESD) generator in the contact mode are numerically simulated using the finite-difference time-domain method. At first the static field is established. Then the conductivity of the relay contact is changed, which initiates the discharge process. The simulated data are used to study the effect of design choices on the current and fields. They are compared to measured field and current data using multidecade broadband field and current sensors. The model allows accurate prediction of the fields and currents of ESD generators, thus it can be used to evaluate different design choices.

Index Terms—Electrostatic discharge (ESD) generator, field sensors, finite-difference time domain (FDTD), numerical modeling, numerical simulation.

I. INTRODUCTION

ROBUSTNESS toward electrostatic discharge (ESD) is tested using ESD generators. Most generators are built to meet the specifications spelled out in IEC 61 000-4-2 [1]. Insufficient specifications contribute to problems in reproducing test results if a different brand ESD generator is used [2], [3], [4], [5]. For that reason, the IEC TC77b presently discusses changes to these specifications.

ESD can disturb systems by its current and the associated electric and magnetic fields. While the current is somewhat specified there is no specification for the fields. Presumably, it had been assumed that a specification for the current at the discharge tip would sufficiently define the transient fields. Presently, the design of ESD simulators follows mostly a trial and error path. The goal is a current defined by a 0.7–1-ns rise time and 3.75-A/kV peak value for contact mode discharges. Since there are no field specifications, the electric (E) and magnetic (H) fields may vary significantly from simulator brand to simulator brand although the currents are somewhat similar [5].

Two discharge modes are used in ESD testing: an air discharge mode and a contact discharge mode. A spark between the tip and the ground initiates the discharge in the air discharge mode. The mostly linear response of the simulator's lumped components and the nonlinear arc determine the current. In this case, the simulator current can be modeled using the impedance as seen from the ground plane into the discharge tip. This impedance can be transformed into the time domain

as the impulse response and convolved with the nonlinear arc characteristic [6], [7]. This yields the discharge current. Fully modeling the arc via differential equations in a time stepping algorithm is in principle possible, but may require additional measures to avoid divergence, as the ionization equations are highly sensitive to errors in the electric field across the gap [8]. Other approaches are given in [9].

Many publications show a strong interest in simulating ESD or the coupling of ESD into circuits and enclosures. In most simulations a user given ESD current was used [10], [11]–[14]. It was either obtained from the standardized waveform or from measured data.

A numerical model based on standard finite-difference time-domain (FDTD) method using Yee cells was presented by Angeli and Cardelli [13], the ESD discharge current was obtained from measurements and a mathematical model. It was inserted into the discharge channel. A numerical model based on a FDTD formulation with impedance boundary conditions was developed by Maradei and Raugi [14]. This method avoided the large number of cells required by the standard FDTD method otherwise needed in modeling media with limited conductivity. The fields radiated during the ESD discharge phase were studied by this FDTD impedance network boundary conditions (FDTD-INBCs) model. The effect of ferrites on ESD currents and fields was studied by [12].

Obtaining the current and the fields just from the charging voltage and the geometry was achieved for highly simplified structures in [8] for air discharge, i.e., including the nonlinear arc in a full-wave model.

Leuchtmann and Sroka [10], [11] obtained the transient fields of ESD simulators using the generalized multipole technique. The model contained parts of the simulator geometry but used a measured current as the excitation method. The measured data presented in [11] used the same field sensors but the deconvolution of the low-frequency rolloff had not been implemented at that time.

This work obtains the current and fields from an ESD simulator using only the geometry and the charge voltage. The ESD generator is used in the contact mode. In the contact mode the discharge is initiated by a gas breakdown in a relay, i.e., there is no arc to ground at the tip of the generator such as there is in air discharge mode. The resistance drop in the relay is a user given function that is much faster than the 0.7–1-ns rise time observed in the discharge current. The conductivity can change from zero to infinity in one time step. To follow the physical stages of charging and discharging as close as possible, the ability to handle time-dependent material properties has been introduced
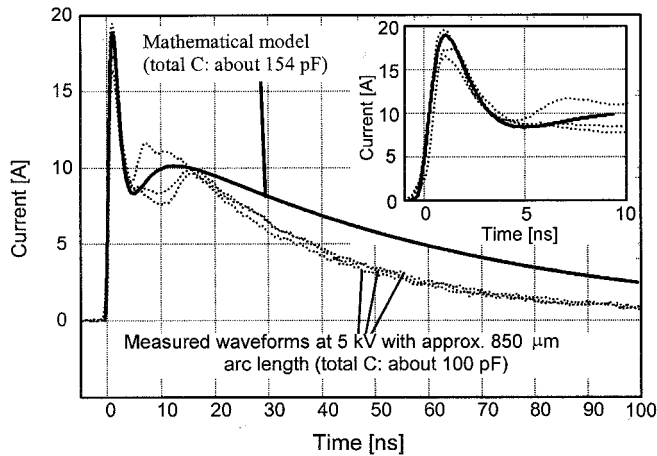
Fig. 1. Mathematical reference waveform compared to measured human-metal ESD waveforms. Human-metal ESD at 5 kV having arc lengths of about 0.85 mm.

into the FDTD algorithm. It is used to model the switching of the high-voltage relay as well as to speed up the process of stabilizing an electrostatic field prior to the discharge.

The main advantage of this method relative to previous work is the ability to predict the discharge current and the related fields just based on the geometry and the charging voltage.

Section II of this paper provides a general analysis of an ESD generator. The specific ESD generator modeled and the numerical approach are explained in Section III. Section IV explains the measurement setup used. Simulation results are presented in Section V and issues of convergence are discussed in Section VI.

II. GENERAL ANALYSIS OF ESD GENERATOR CURRENTS

A. Discharge Current

The aim of an ESD generator is to reproduce typical human-metal ESD. Historically, a peak value of 3.75-A/kV and 0.7–1-ns rise time have been defined as a typical human-metal ESD. Such a discharge is typical for moderate humidity and typical speed of approaches at 5 kV for a human-metal ESD event [7]. Reproducibility always has been an issue. But if an object or a human is discharged multiple times using the same voltage, the discharge current will repeat quite well for those discharges that have the same arc length [7]. Analyzing data from measured human-metal ESD at 5 kV shows that discharges having 0.85 mm arc length will be close to the peak current and rise time values defined by the standard (Fig. 1). Based on these waveforms a mathematical approximation has been derived. It is the reference current throughout this paper. Its values have been chosen to match the standardized values as close as possible: 0.85 ns rise time, 3.75 A/kV peak value, 2 A at 30 ns, 1 A at 60 ns, about 150 pF total capacitance, decay time constant about $330\,\Omega * 150$ pF.

The reference waveform is given by

$$i(t) = \frac{i_1}{k_1} \cdot \frac{\left(\frac{t}{\tau_1}\right)^n}{1 + \left(\frac{t}{\tau_1}\right)^n} \cdot \exp\left(\frac{-t}{\tau_2}\right) + \frac{i_2}{k_2} \cdot \frac{\left(\frac{t}{\tau_3}\right)^n}{1 + \left(\frac{t}{\tau_3}\right)^n} \cdot \exp\left(\frac{-t}{\tau_4}\right)$$

with the following constants:

$$k_1 = \exp\left(-\frac{\tau_1}{\tau_2}\left(\frac{n\tau_2}{\tau_1}\right)^{1/n}\right)$$

$$k_2 = \exp\left(-\frac{\tau_3}{\tau_4}\left(\frac{n\tau_4}{\tau_3}\right)^{1/n}\right)$$

and the following parameter values:

$I_1 = 21.9$ Amp	$\tau_1 = 1.3$ ns	$\tau_3 = 6$ ns	$n = 3$
$I_2 = 10.1$ Amp	$\tau_2 = 1.7$ ns	$\tau_4 = 58$ ns	

This reference waveform is still under discussion within the IEC TC77b but may be part of the next IEC 61 000-4-2 standard. In contrast to double or quadruple exponential waveforms this waveform provides a physical, finite current derivative. The current rises smoothly after $t = 0$. Gardner [15] first published this formulation applying it to lightning strokes.

B. Ground-Strap Current

The human-metal ESD discharge current is understood as the superposition of two currents: The initial peak current initiated by the charges on the hand-metal structure and the later, slower waveform caused by the charges on the surface of the body (body-waveform). In an ESD generator, the body waveform is obtained from the discharge of the components in group 3, as shown in Fig. 4. One would expect that the initial peak current is driven by the distributed capacitance between the generator tip and the ground plane. But most generators exhibit only a small electrostatic field on their outside. Via the ground strap they carry a local ground potential into the structure and most of the capacitance that creates the initial peak can be found between the internal high voltage carrying parts of the generator and the local ground. The charges have to return via the ground strap, but the connection between the local ground (battery and electronics of the ESD generator) and the ground strap can be constructed such that high frequency components are hindered from passing from the local ground onto the ground strap.

III. ESD GENERATOR MODELED AND THE NUMERICAL APPROACH

A. ESD Generator Modeled

A modified commercial ESD generator was selected to verify the numerical modeling techniques. The modified generator was built based on the commercial generator but with a new discharge head which was made of a high-voltage relay, capacitors, resistors, etc. as is shown in Fig. 4. Its discharge current waveform had been modified to improve the match to the reference current waveform, Fig. 3. Fig. 2 shows the modified ESD generator. The newly designed discharge head is composed of the discharge tip, a pulse forming filter, a high-voltage relay, two copper rings, a 330-Ω resistor and a 110-pF capacitor as chosen by the manufacturer.
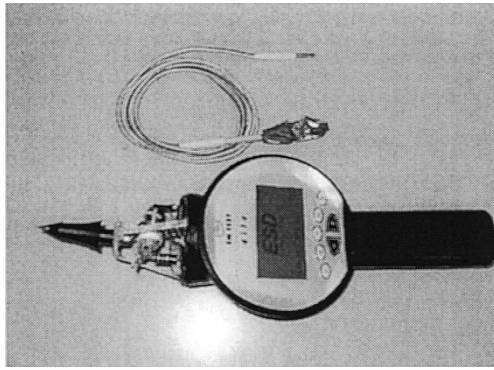
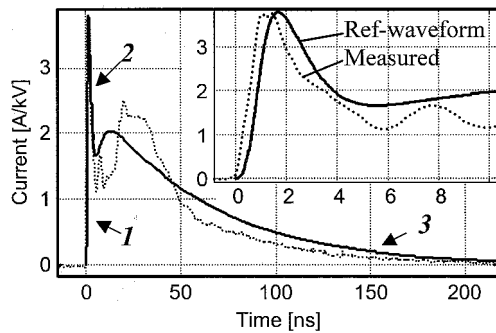Fig. 2.   ESD generator with modified discharge head.

Fig. 3.   Comparison of the reference waveform with the measured discharge current of the modified generator. The numbers signify different parts of the waveform. 1) rising edge; 2) falling edge; and 3) slow falling edge.


(a)

(b)

Fig. 4.   (a) Equivalent circuit of the generator. (b) Photograph of the discharge module.

Although the discharge current of this modified generator is quite smooth, it still exhibits more ringing than the reference waveform, Fig. 4. An equivalent circuit of the generator is shown in Fig. 4. It was not used to calculate the current, but it aids in understanding the main physical processes and the numerical model of the generator. The values of C2, C4, and C5 have been optimized for achieving a reasonable current. It does not include all parasitic capacitances and inductances, e.g., the capacitance across the relay and some of the distributed capacitances of the wiring. It needs to be pointed out that it is only intended to illustrate the main physical processes.

The components can be divided into three groups. Each group is associated with one part of the discharge waveform. The value of each component is shown in Table I. There is a resistively connected (R2) copper-ring structure (C2, C4) covering the generator's discharge module. It is discussed in detail in the later part of this paper. Limited by the resistor R2, the ring capacitance increases the initial current peak. The photo in Fig. 4 shows the discharge head after removing the copper-ring structure (C2 and R2). The capacitor C4 is associated with the electric field between the copper-ring structure (on high-voltage potential) and the ground. The capacitor C5 is the capacitance between the body of the generator (on a low-frequency ground via the ground strap) and the ground plane. Both form the displacement current return for the initial peak and influence the rise time and the current peak value.

Without this rise time forming filter, the discharge current would rise in less than 200 ps, as it would be determined by the voltage collapse within the high-pressure Sulfur Hexa Floride[6]
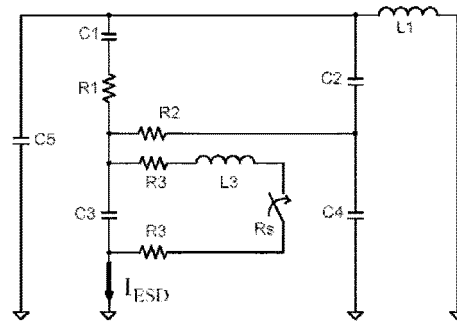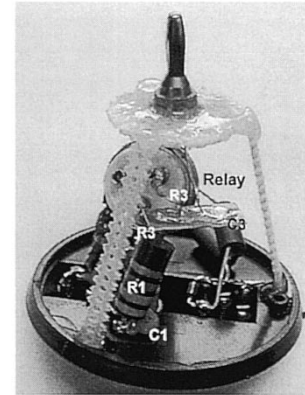
filled relay. The frequency dependence of the dielectric materials (FR-4, Capacitor) is sufficiently small within the frequency range of interest that it does not need consideration in this simulation.

The ESD generator model was simulated using either a short ground-strap computational domain or a long ground-strap computational domain. The short ground-strap computational domain was setup to simulate the 80-cm-long ground strap while the long ground-strap computational domain was used to simulate the 200-cm ground strap. The long ground-strap domain needs four times more simulation time than the short one. The smaller computational domain was used to study the boundary conditions, the domain size and the effect of the copper-ring structure. The larger domain was used to study the current and the transient field.

B. Numerical Approach

The FDTD method was used. Relative to [10] and [11], this allows predicting the current and fields from an ESD generator using only the geometry and the charge voltage. EZ-FDTD, a program created by our group, and a commercial FDTD package [18] were used. The access to the source code allowed implementing the time-dependent media in the EZ-FDTD code. Later, Zeland software introduced this option for Fidelity on our request. In contrast to EZ-FDTD, Fidelity allows a nonuniform grid.

The calculation time and the memory size set a lower practical limit on the amount of detail that can be modeled. The FDTD

TABLE I
COMPONENT VALUES IN THE EQUIVALENT CIRCUIT

|	Component	Value	Function	Modeling method
Group 1 Rise-time	C3	20 pF, PCB board	Pulse forming R-C-R filter, L3 is its loop inductance	C: Two metal layers with dielectric material in between
	R3	36 Ω, lumped		R: Single cell, σ = 13.9 S/m.
	L3	About 6 nH, distributed	Loop inductance	The loop's geometry is part of the ESD generator geometry model.
	C4	In the SPICE model 15 pF, distributed	Capacitance between discharge tip and ground plane.	The geometry model includes the structural elements.
	C5	In the SPICE model 20 pF, distributed	Capacitance between the simulator body and the ground plane.	The geometry model includes the structural elements.
Group 2 Pulse width and height	C2	In the SPICE model 5 pF, distributed	Influences the width of the initial pulse	This capacitance is simulated by the structure itself.
	R2	120 Ω, lumped		Single cell, σ = 0.9 [S/m].
Group 3 Falling edge	C1	110 pF, lumped	Determines the tail of the waveform. L1, the ground strap loop inductance, is estimated to be 3500 nH (rectangular loop assumption).	C: Two metal layers with dielectric material in between
	R1	330 Ω, lumped		Single cell σ = 0.756 S/m
	L1	3500 nH, distributed		The ground strap is included in the numerical model geometry.
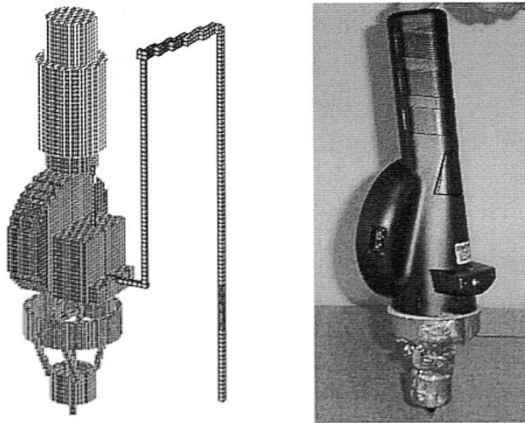
Fig. 5. 3-D view of the model, using a short ground strap and the ESD generator using Fidelity [18].

model includes the physical geometry of the generator, the relay, pulse forming filter, ground strap and lumped elements. For Fidelity, the cell size varies from 2 mm within the generator, to 10 mm at the boundary, the typical domain size being 120 × 120 × 55 cm. Larger and smaller domains have been used for investigating the convergence of the result.

In EZ-FDTD, the cell size is set to 3.175 mm and the domain size is 184 × 70 × 50 cm terminated by second-order perfectly matched layer (PML). Fig. 5 shows the three-dimensional (3-D) view of the model.

Figs. 6 and 7 give details of the model, while Table I and the equivalent circuit of Fig. 4, explain the functionality of the circuit and its components. In Fig. 7, part of the copper (CO) ring structure is removed to allow viewing of the inside.

The switch of the relay is built as a single cell. The material's conductivity is set to zero during the charging phase. After sufficient stabilization of the electrostatic field, the conductivity is set to infinity to initiate the discharge. Fig. 8 shows the details of the high-voltage relay. The dielectric layer in this figure is to simulate the capacitance between the switch and the relay body. The capacitance values have been measured for the Kilovac HC-5 relay, which is about 2 pF.

As discussed in the measurement section, an improved ESD current target was used to measure the discharge current. The difference in current between discharging into a large ground plane relative to discharging into the current target is less than 2% for the peak value due to the low input impedance of the current target. This and the flat frequency response allowed excluding the target from the numerical modeling geometry.

C. FDTD Handling of Time-Dependent Media

The ability to handle time-dependent material was introduced into the FDTD code. The EZ-FDTD code was modified such that the material parameters are a function of time. In this way, the physical process of charging and discharging can be modeled accurately. The flowchart of the algorithm is shown in Fig. 9.

The process is as follows.

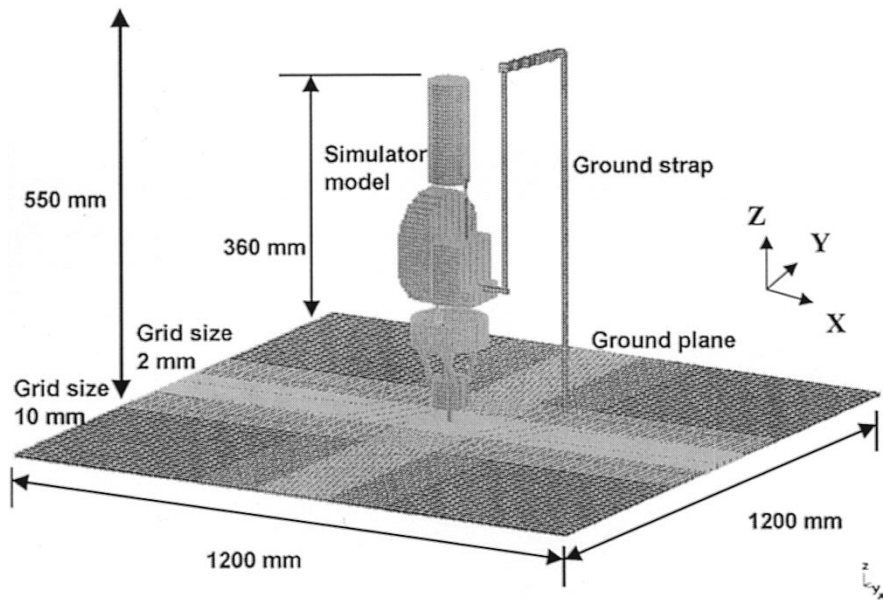1) The material properties and their time history are given by the user before program start.

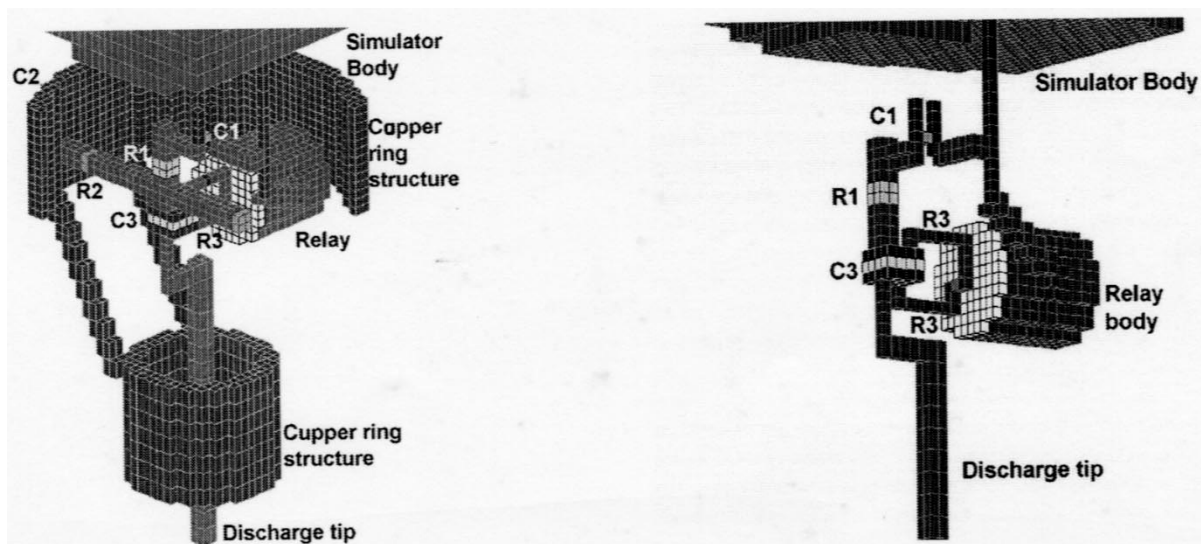Fig. 6.   Model and computational domain of the short-ground-strap (80-cm-long) domain.

Fig. 7.   Structure of the model in detail, and with no copper ring.
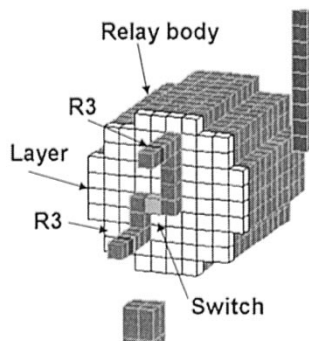

Fig. 8.   Detail of the high-voltage relay. The layer in this figure is a dielectric layer.

2) In every time step the program checks the time histories to determine if the material properties need to be changed.

3) If so, the present E and H fields are stored, the material is updated and the previous E and H fields are applied to the modified geometry as initial start values.

4) The fields are updated using the usual FDTD update equations, then step 2) to 4) are repeated.

This may apply a nonphysical solution to a geometry, for example, fields within a perfect electric conductor. In such cases it may initiate a few time steps of ringing to establish the new geometry. Instabilities have not been observed for the structures investigated.

D. Charging Phase

Different methods exist to charge the generator's geometry and capacitors prior to the discharge. One option is to use an electrostatic field calculation prior to the FDTD code and to import the field distribution as initial condition. The advantage of
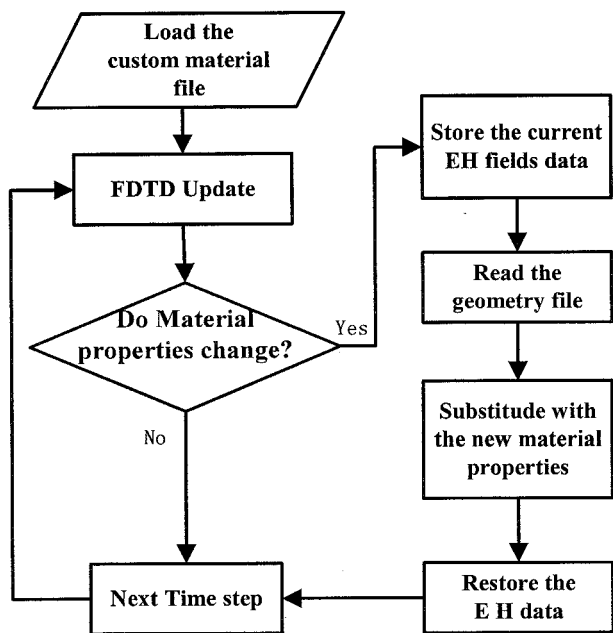
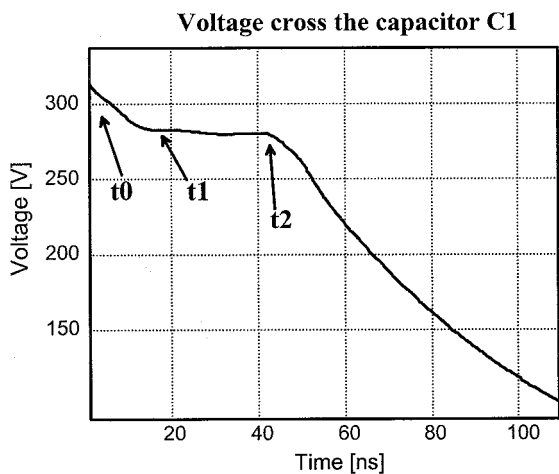Fig. 9. Flowchart of the EZ-FDTD ESD generator model.
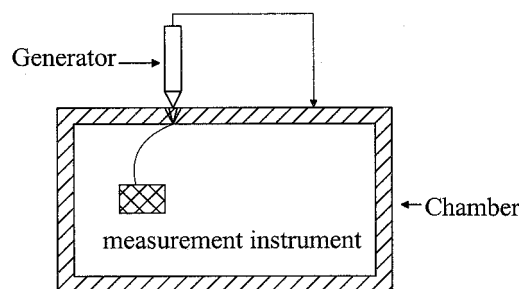

Fig. 10. Voltage across the capacitor C1.

Fig. 11. Diagram of the measurement setup. Dimensions of the chamber are $3 \times 3 \times 4$ m.

peak discharge current the structure is considered to be ready for discharging. The method is depicted in Fig. 10.

Phase 1) Charging (Time: t_0–t_1)

A predefined E field is inserted into the capacitor. During this phase, the charges diffuse from the capacitor plate to the whole system until the system achieves balance.

The method did not yield unstable results providing lossy conductive material was introduced during the stabilization phase. As such, the conductivity of the metallic parts was reduced to 2.0 S/m only during the stabilization phase.

Phase 2) Stabilization (Time: t_1–t_2)

The current in the discharge head and the ground strap decay to zero.

Phase 3) Discharge (Time: t_2–t_{final})

The system is stable now. The conductivity of the switch in the high-voltage relay is set to infinity, the discharge current starts to flow.

The method used in this simulation follows along the physical process of charging and discharging.

Using the Fidelity time-domain code, the structure is charged by a 1-ns full-width-at-half-maximum (FWHM) Gaussian current pulse that is introduced by a line source connected to the 110-pF capacitor. It is attached via two lossy wires (small vertical wires to the right of the label "C1" in Fig. 7). To accelerate the stabilization of the electrostatic field, the conductivity of the metallic structures is set to 500 S/m. Before the discharge phase, the conductivity is set back to 2×10^8 S/m.

Fidelity needs between 4000 and 8000 time steps (3.66 ps per time step) until the field is sufficiently stable. Depending on the domain size and the boundary conditions, calculation times vary between 15 min and 8 h on a 2.2-GHz PC. There were eight million cells in the largest calculations. EZ-FDTD needs between 8000 and 26 000 time steps (5.09 ps per time step) until the precharge field is sufficiently stable. For the large domain having 20 million cells, the calculation time was 60 h on a 2.2 GHz PC.

IV. MEASUREMENT SETUP

Field and current sensors were mounted on the wall of a $3 \times 3 \times 4$-m shielded room. The generators are discharged on the outside of the room while the instrumentation is within the shielded room. This prevents coupling into the instrumentation or their cables, Fig. 11.
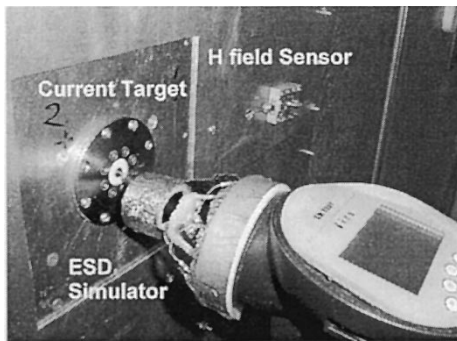
this method is that no time steps are used to establish charged conditions. The disadvantage is that the electrostatic calculation would use an infinite region while the FDTD domain is truncated using PML or other boundary conditions. Thus, there may be a nonphysical initial conditions that again need time steps to tranquilize.

Another approach is to charge the model using e.g., a Gaussian pulse source. In this case it will take many time steps to stabilize the electrostatic field. Once it is stabilized, the conductivity in the relay is changed to infinite, initiating the discharge. This method requires more time steps than the first but it is easier to implement, as no external electrostatic calculation is needed.

For the EZ-FDTD code, a mixed method is used: First an electric field is inserted between the two metal plates of the 110-pF capacitor. Then, the model needs some time to charge the other parts of the circuit. After about 40 ns, the system is fully charged. If the currents have subsided to about 5% of the

Fig. 12.   Current target and *H*-field sensor on the wall of the shielded room.
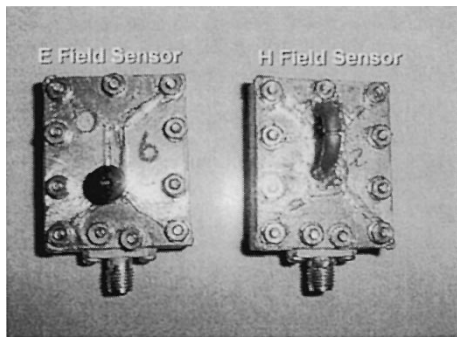

Fig. 13.   Electric and magnetic field sensors. The active circuits are powered through the RF connection.

The generator is operated in the contact mode. The discharge currents and fields are normalized to 1 kV charge voltage.

A. Current Target

Due to insufficiencies of the Pelligrini target [16], [17] for measurements above 1 GHz, an improved current target was used. The frequency response of the target-attenuator-cable chain is within ± 0.3 dB up to 1 GHz and ± 0.8 dB up to 4 GHz [16], [17]. The input impedance of the target can be modeled by a 2-mm-long 50-Ω transmission line terminated with 2 Ω [10], [11]. A source impedance of 266 Ω is obtained from the standardized peak value of 3.75 A/kV. Relative to this impedance the target can be considered as a very good short circuit, thus the measured current values can be directly compared to the simulated current values. The simulation discharges the generator into a large metallic plane not containing the 2-Ω current target. The overall current measurement error will be dominated by the uncertainty in the voltage gain of the oscilloscope, not by the target-attenuator-cable chain.

B. Field Sensors

The field sensors are ground based field sensors with active integration using a GaAs impedance converter for the *E*-field sensor and a multistep analog integration for the *H*-field sensor. They are rectangular in shape and are about 4 cm by 3 cm by 1 cm.

See Figs. 12 and 13. When measured in an open strip line, they exhibit a ± 1.5 dB frequency response from 2 MHz to 2 GHz (Figs. 14 and 15). The measurement was performed for different positions within the strip line and yielded results within ± 1 dB.
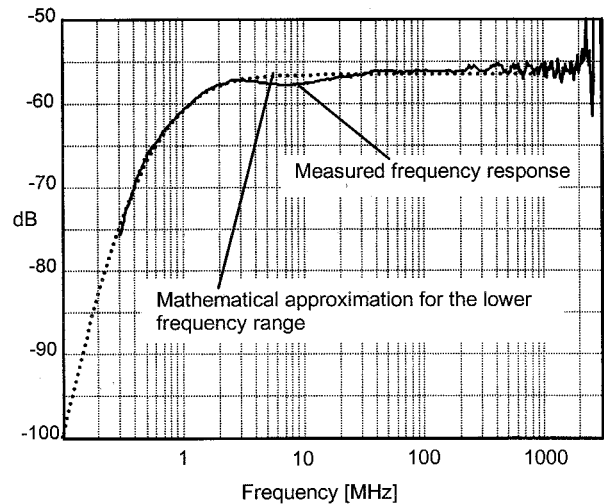

Fig. 14. Frequency response of the *H*-field sensor measured in an open strip-line (solid) and a mathematical approximation (dotted) of the low-frequency rolloff.
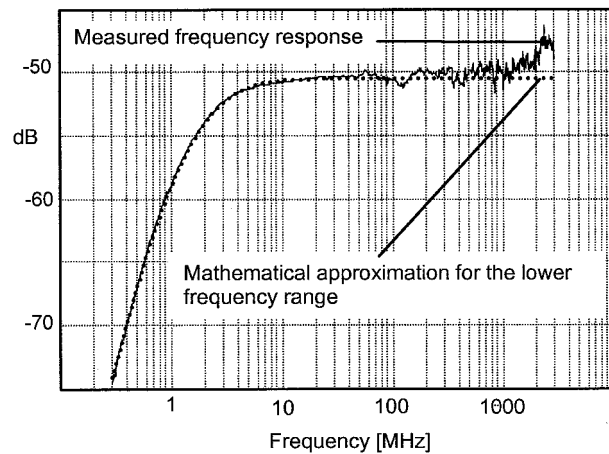

Fig. 15. Measured frequency response of the *E*-field sensor and a mathematical approximation of the low-frequency rolloff.
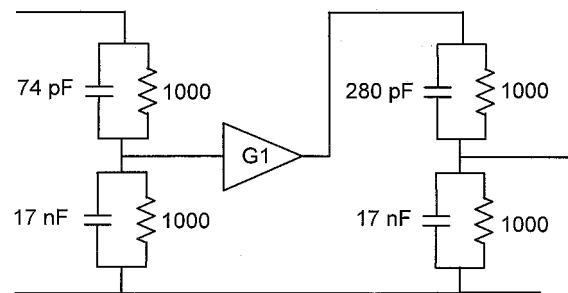

Fig. 16.   Circuit describing the compensation function for the *E*-field sensor. For the *H*-field sensor a circuit having four such networks have been used.

Although the sensors are rather broadband, there is a negative effect caused by the lower frequency rolloff. For the first few nanoseconds, the sensor output voltage is proportional to the field. But within a few nanoseconds, the effect of the low-frequency rolloff starts to be visible (Fig. 18). To compensate for that, a deconvolution was introduced (Figs. 14, 15 and 18).

The compensation function of the lower frequency response can be explained using the circuit shown in Fig. 16.
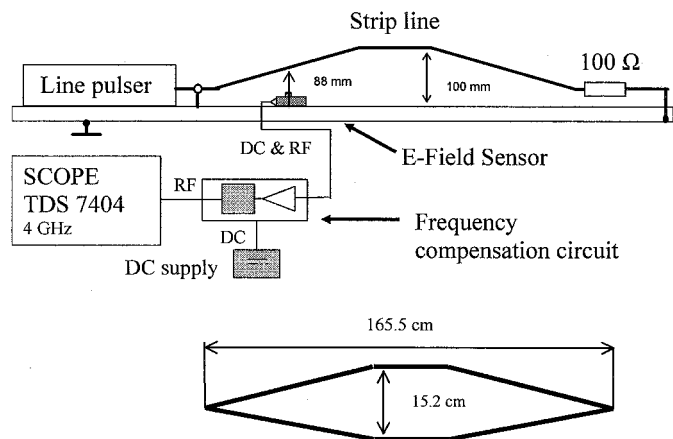
Fig. 17. Open strip-line cell and the deconvolution setup for the *E*-field sensor. The strip line maintains 100 Ω.

Fig. 19. Top view of the computational domain for the short ground strap. Ground-strap length 0.8 m is the total length which includes the vertical part perpendicular to the ground plane.
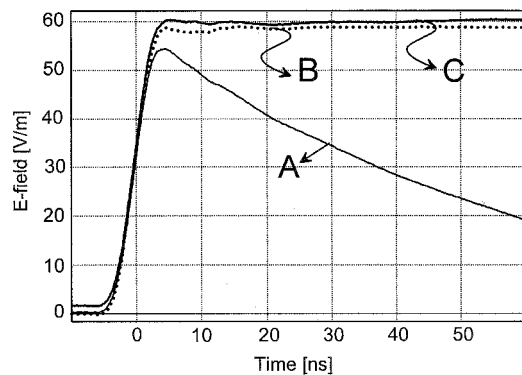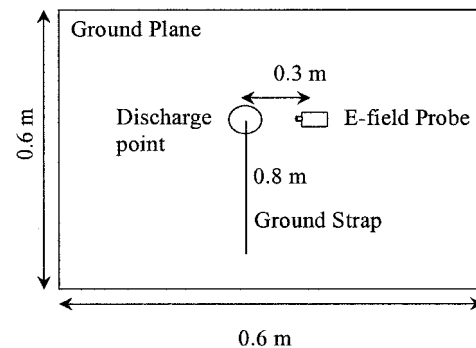

Fig. 18. Deconvolution of the *E*-field data output. (a) Signal obtained by dividing the sensor output voltage by a calibration factor of 180 μV/(V/m). (b) Expected field strength in the cell, derived from the cell dimension and the injected step function. (c) Field strength obtained by deconvoluting the sensor output voltage.
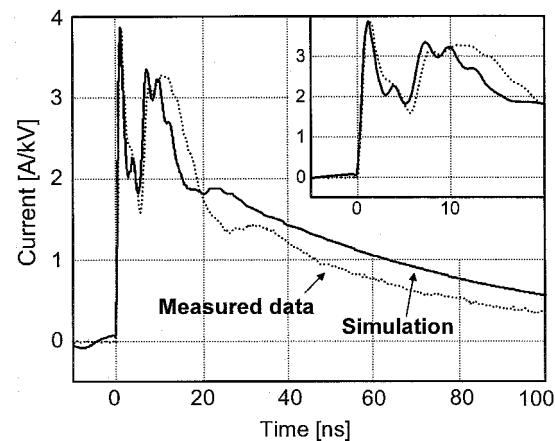

Fig. 20. Comparison of simulated and measured discharge currents for the short ground strap. Time scale has been set to zero at the moment of the relay switching.

Deconvolution using measured impulse responses would introduce additional noise into the data, as the noise of the measured impulse response would be added to the noise in the data. For that reason the low-frequency rolloff was approximated by a cascaded first-order high-pass filters having different 3-dB frequencies.

To verify the deconvolution method, a square wave was injected into a strip line structure (Fig. 17). Both the waveform from the pulse generator and the sensor output voltage were measured. The output of the *E*-field sensor and the result of the deconvolution are depicted in Fig. 18.

After deconvolving, the original *E* field can be obtained (Fig. 18). A similar deconvolution algorithm was implemented for the *H*-field sensor. The useful time window for the field measurements is between 0.2–about 100 ns. The lower limit of 200 ps is given by the upper frequency response of the sensors. The upper limit of 100 ns is determined by the dynamic range limit of the time-domain data, any offset in the time-domain waveform and by the sensitivity of the deconvolution to any inaccuracies in the frequency response of the sensor.

V. SIMULATION RESULTS

During all the measurements, the ESD generator was supported by Styrofoam to minimize the influence of the human body on the currents and fields of the ESD generator.

1) Simulations Using a Short Ground Strap: To reduce computation time while being able to test the validity of the model of the generator, a short ground strap of 0.8-m length was used during this set of simulations and measurements. The computational domain is shown in Fig. 19.

Fig. 22 shows the location of the *E*-field and *H*-field probing points, relative to the ESD generator and its ground strap. The sensor have not been numerically modeled, instead the numerical simulation recorded the field strength at that location.

The discharge head in this simulation model used a 330-Ω resistor and a 150-pF capacitor, while the actual ESD generator has a 110-pF capacitor. For that reason the current decays slower in the simulation than in the measurement.

The discharge current, shown in Fig. 20, and the electric field at a distance of 0.3 m, shown in Fig. 21, agree with the measurements. Especially, the initial part of the waveform, that most often determines the equipment's response to an ESD, is modeled well.

2) Simulations Using the 2-m-Long Ground Strap: The original ground strap of the ESD generator is 2-m long. The
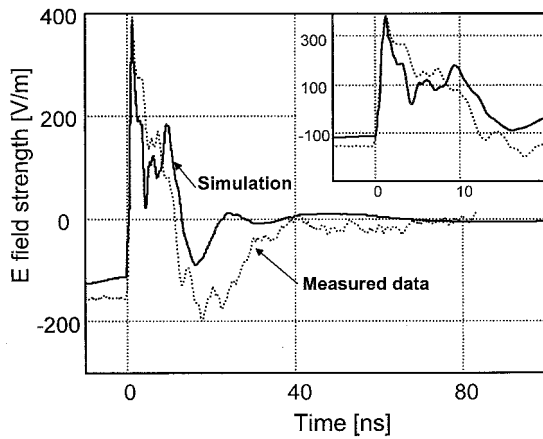
Fig. 21. Comparison of simulated and measured *E*-field strength, 30 cm away from the discharge point. An 80-cm-long ground strap was used in the simulation.
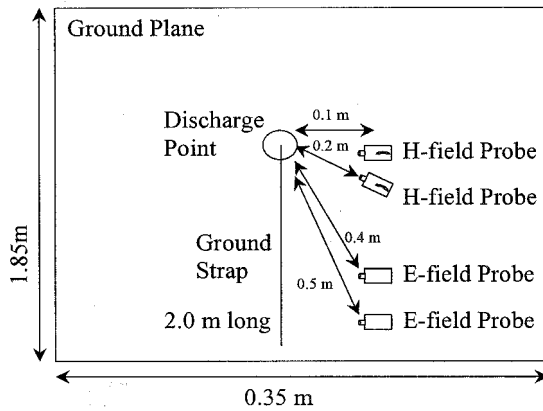

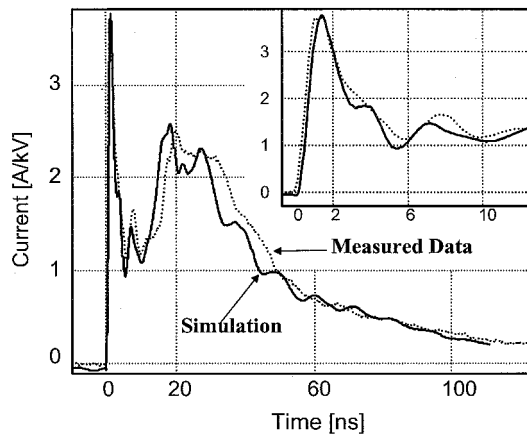Fig. 22. Top view of the EZ-FDTD computational domain of the 2-m-long ground strap.

Fig. 23. Comparison of simulated and measured discharge currents.

computational domain used for the long ground strap is shown in Fig. 22.

Fig. 22 shows the location of the *E*-field and *H*-field probing points relative to the ground-strap position. The discharge current was simulated and compared with the measured data in Fig. 23. The current in the ground strap was also simulated and compared with the measured result. The transient *H*-field data at 10- and 20-cm distance from the discharge point were simulated
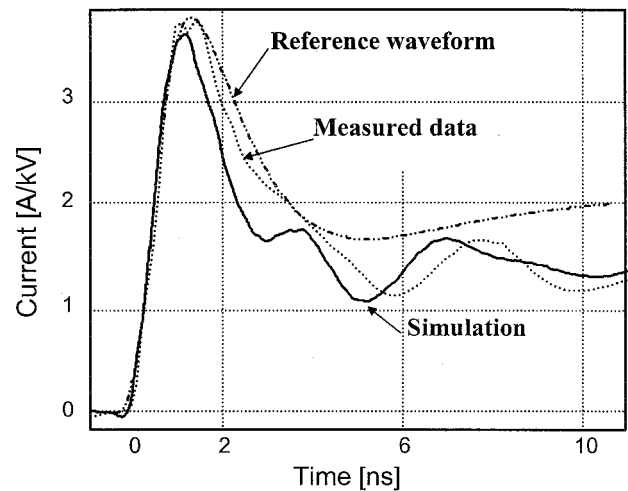

Fig. 24. Discharge current during the first 10 ns. The reference waveform in this figure is the mathematical reference waveform from Fig. 1.

TABLE II
COMPARISON OF THE RESULTS

	Measured data	Simulation
Rise time	0.8 ns	0.8 ns
1st peak current	3.74 A/KV	3.77 A/KV
2nd peak time	19.8 ns	18.5 ns
2nd peak current	2.51 A/KV	2.55 A/KV

and compared with the data measured by the *H*-field sensor. The transient *E*-field data at 40- and 50-cm distance from discharge point was simulated and compared with the data measured by the *E*-field sensor.

The measured and simulated discharge currents (Fig. 23) show good agreement. The small oscillations on the later part of the simulated waveforms are most likely a result of modeling the electronics and the battery as metallic blocks.

It is known from the evaluation of shielding that electronic circuit boards reduce the Q factor of enclosures. Based on that, it is reasonable to conclude that modeling the electronic parts, battery, display and the interconnecting wires would introduce additional losses leading to a reduction of oscillations.

The discharge pulse in the first 10 ns is compared with the measured data in Fig. 24.

The result of the simulation is compared with the measured data in Table II. The simulation result is low-pass filtered using a second-order 1.5-GHz filter to yield a bandwidth similar to the measurements.

The spectral density of the discharge current is also compared in Fig. 25.

As shown in Fig. 25, the spectral densities of the currents are quite similar. Note that above about 1 GHz the measured data is dominated by the dynamic range limit of the oscilloscope.

A. Ground-Strap Current

The ground strap is needed to provide a low-frequency discharge path, but the ground strap should not conduct any of the fast rising initial current of the ESD discharge. If it does, it would introduce field components that do not reflect the human-
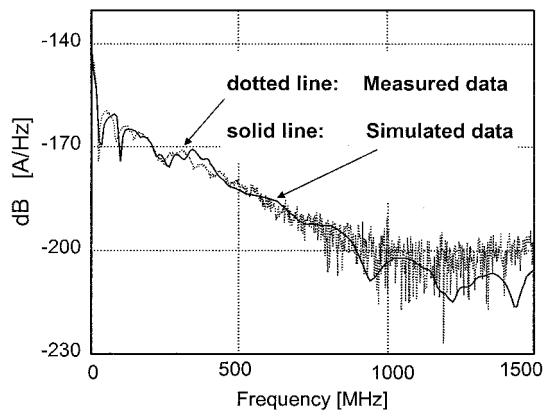
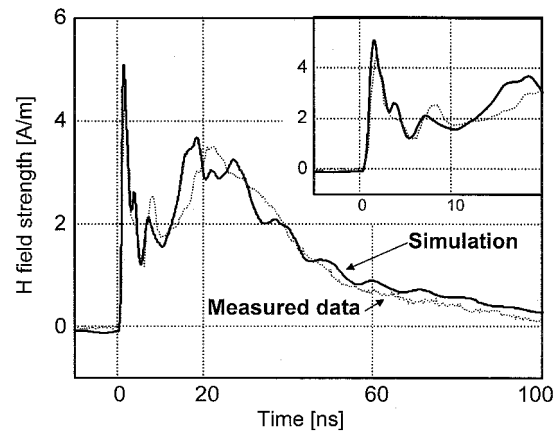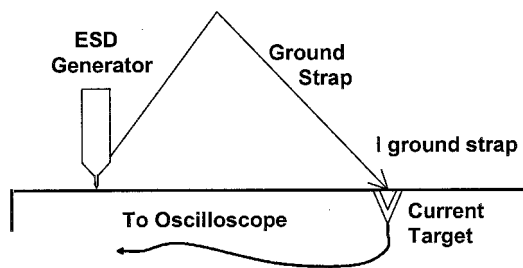Fig. 25.   Discharge current spectral density comparison between the measured data and the simulation.

Fig. 26.   Setup to measure the ground-strap current.
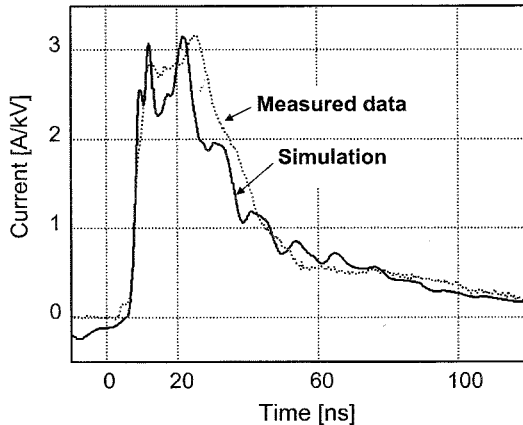
Fig. 27.   Comparison of simulated and measured discharge currents in the ground strap.

Fig. 28.   Comparison of simulated and measured *H*-field strength, 10 cm away from the discharge point.

Fig. 29.   Comparison of simulated and measured *H*-field strength, at a distance of 20 cm from the discharge point. See Fig. 22 for the locations of the field sampling points, the generator and the ground strap.

metal ESD as the fast rising current components are attenuated and radiated as they travel along the arm of a human. The ground-strap current can be measured by multiple methods, e.g., a current clamp. But due to the well established frequency response of the current target it is preferable to use it to measure the ground-strap current. This measurement was done by inverting the positions of the simulator and the ground strap on the wall of the shielded room (Fig. 26).

The simulation result of the discharge current in the ground strap is compared with the measurement in Fig. 27.

The discharge current in the ground strap is expected to have less high frequency component compared with the discharge current at the discharge tip, since some of the high frequency
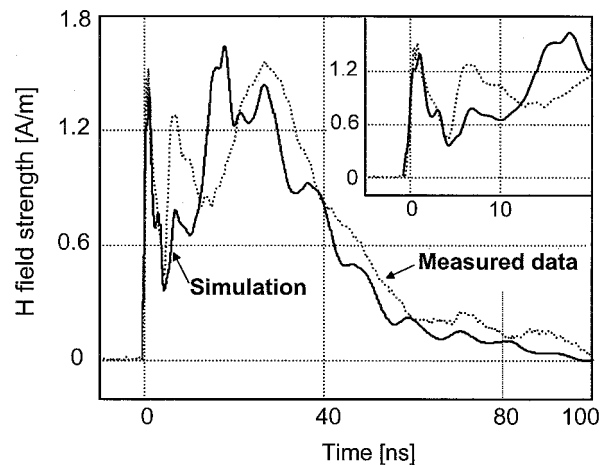
current flows through the parasitic capacitance around the tip. Comparing Figs. 23 and 27 shows that this expectation is fulfilled. Figs. 28 and 29 provide *H*-field simulation results compared to the measured data.

All measurements have been done on the ground plane due to the sensors used.

The transient *E* fields 40 and 50 cm away from the discharge point are simulated and compared with the measured data in Figs. 30 and 31, respectively. The figures show that the simulation results agree well with the measured data for the first 20 ns.

The low-frequency component of the simulated *E* field shows considerable larger differences than the initial transient. This might be caused by one of the following reasons: 1) in the measurement, the electrostatic field is strongly influenced by the way the simulator is held and the exact position of the ground strap; and 2) in the simulation, the electrostatic field is strongly influenced by the position of the ground strap and the size and location of parts that hold the initial charge voltage.

However, most failures in electronic equipment is related to fast changing components, such that we do not consider the differences in the slow components as a major drawback for designing ESD generators using based on numerical simulation.
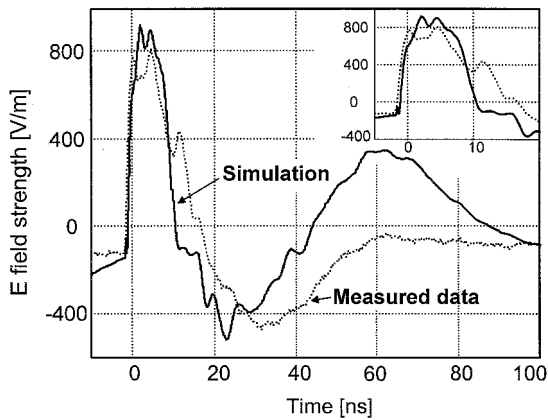
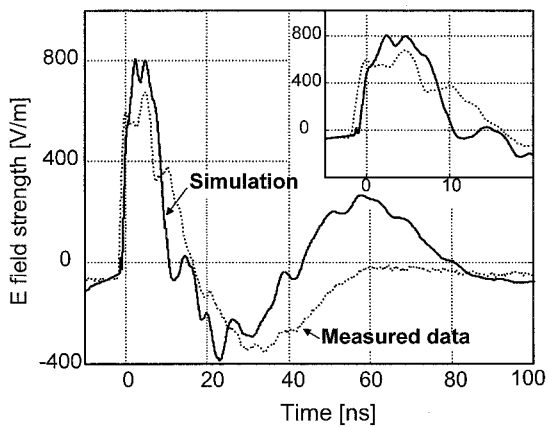Fig. 30. Comparison of simulated and measured E-field strength, 40 cm away from the discharge point.

Fig. 31. Comparison of simulated and measured E-field strength, 50 cm away from the discharge point.

VI. NUMERICAL CONVERGENCE AND MODELING ERRORS

Every measured or simulated result is the superposition of the underlying physical process, the process that we are interested in, noise and other errors introduced by the simulation or measurement technique and setup. Without knowing the ratio between the data and the superimposed noise, measured or simulated data are of little worth.

ESD is a broadband process. It reaches from static fields to currents having a 100-ps rise time within the relay and the pulse
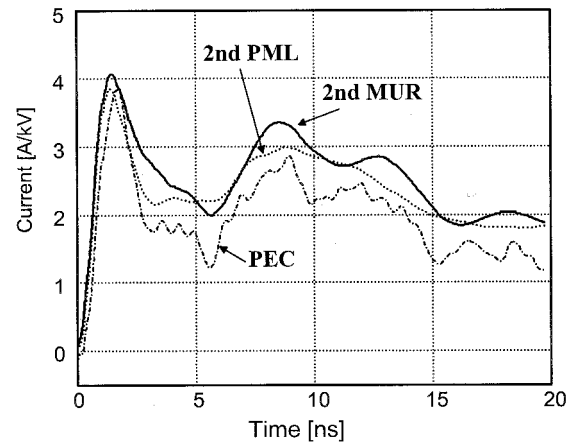

Fig. 32. Effect of different boundary conditions using a smaller domain size of $0.6 \times 0.6 \times 0.55$ m, the Fidelity code, 2–10-mm grid, and a ground-strap length of 0.8 m.
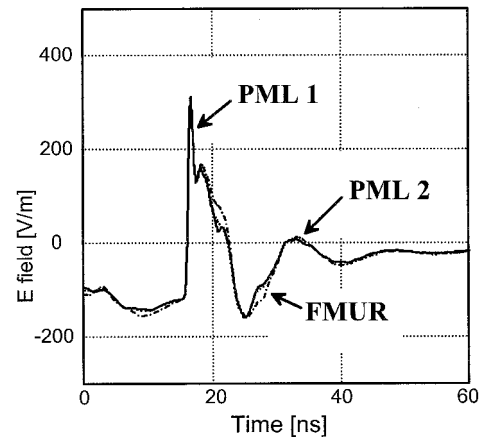

Fig. 33. Effect of different boundary conditions on the E-field strength simulation using a larger domain size of $1.3 \times 1.3 \times 1.0$ m, the Fidelity code, 2–20-mm grid, and a ground-strap length of 0.8 m. The E field is the E-field strength 30 cm away from the discharge point.

Since the field at the ground plane and current data matched well to the simulations, thus suggests that the fields above the ground strap and the current in other parts of the generator might also be predicted with sufficient accuracy.

The reasons for the remaining differences relative to the measurement can most likely be found in the fact that all the electronics, display and the battery of the simulator have been modeled as metallic blocks, not taking their connection inductances and possible losses into account. It was shown that adding inductances into the path could improve the match. Such an inductance was not added in the path as there would have been no other way for obtaining its value than the optimization between measured and simulated results. This would contradict the aim of being able to predict the behavior of an ESD generator.

forming structure. For the rise time and the peak value it is essential to model fine details while other processes have relevant fields that expand through the entire simulation domain. These are the electrostatic field and the fields that relate to the ground-strap inductance. The effect of grid cell size, domain size, and boundary conditions on the current and fields was investigated to establish trust in the solution.

A. Boundary Conditions

If the domain size were infinitely large, the type of boundary conditions would be irrelevant. For the rather small domain size of $0.6 \times 0.6 \times 0.55$ m, the boundary conditions have a significant effect, especially if the less realistic perfect electric conductor (PEC) boundary conditions are chosen. The PML boundary condition reduces the oscillation on the ground strap (Fig. 32), better than the second-order Mur boundary condition. For larger domain sizes, for example $1.6 \times 1.6 \times 0.8$ m, the effect of the boundary conditions nearly vanished providing no PEC has been used.

Fig. 33 shows the effect of the boundary condition on the simulated E field 30 cm away from the discharge point. Here
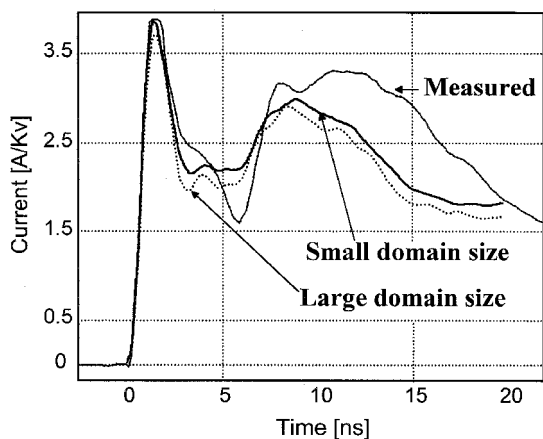
Fig. 34. Influence of the domain size on the calculated results using the Fidelity code, 2–10-mm element edges and 0.8-m ground strap. The small domain is $0.6 \times 0.6 \times 0.55$ m, and the large domain is $1.2 \times 1.2 \times 0.55$ m.

FMUR stands for first-order MUR, PML 1 uses PML but allows to end the ground plane shortly before the absorbing boundary conditions begin while PML 2 continues the ground plane into the PML. Overall, the effect of the boundary conditions on the electric field is weak, indicating that the numerical simulation is trustworthy.

B. Calculation Time

The boundary conditions effect the calculation time significantly

Calculation Time,	PEC	2nd MUR ABC	2nd PML depth 6
2.2 GHz PC	2485 (s)	2576 (s)	8102 (s)

The calculation time is based on a short ground-strap (80-cm long) model and 10 000 calculation steps. Using fourth-order PML and a depth of six grid elements, the Fidelity code runs about 30% faster than EZ-FDTD. The second-order PML was chosen for comparison with EZ-FDTD.

C. Domain Size

The electrostatic field and the magnetic field of the ground-strap current extend through the calculation domain. It has been investigated how the domain size influences the results (Fig. 34).

Fig. 34 indicates that the domain size of $1.2 \times 1.2 \times 0.55$ m is sufficient as the difference between the results is small. At larger domain sizes, the influence of the domain size diminished further.

VII. DISCUSSION

A. Parametric Studies

This simulation method allows investigating the effect of design choices on the construction of ESD generators. It is possible to simulate structures that cannot be built (e.g., test the effect of removing the electronics and the battery). Some of the possible design choices are as follows.
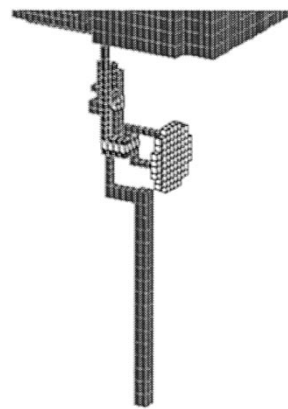

Fig. 35. Discharge tip without copper ring, relay body and its connection to local ground.

1) The voltage drop across the relay is much faster than the 0.7–1-ns rise time specified in the standard. To achieve the specified rise time, pulse forming is used. In our model this was done very close to the relay by using an R-C-R filter. But it can also be done in the discharge tip. Both constructions can yield similar currents at the discharge point. But the fields will be quite different as the rapidly changing current is confined to a small space around the relay if the pulse forming is done in close proximity to the relay. Shielding of the pulse forming structure further reduces the radiation of rapidly changing field components.

2) The ground strap can be isolated from all parts of the simulator by, e.g., a 330-Ω resistor, additional inductances or ferrites. Or parts of the internal structure can be directly connected to some metallic parts inside (local "ground") while they are connected to the capacitor via a 330-Ω resistor. It is expected that these design choices influence the amount of "initial peak" current on the ground strap. No part of the "initial peak" current on the ground strap is desired, as the ground strap is only there to return the discharge current of the lumped capacitor. The ground strap should only carry the "body wave," not the "initial peak" current.

3) Most ESD generators contain electronics. The electronics may be at the high-voltage potential and contribute to the distributed capacitance or it may be at the potential of the local "ground."

4) There are no restrictions on the size of an ESD generator. While it is possible to realize the correct discharge current using a very small ESD generator, it is expected that the fields will be fundamentally different.

5) Some commercial ESD generators exhibit an initial peak current that falls as fast as it rises. The peak negative current derivative approaches the value of the peak positive current derivative. The standard setting bodies intend to regulate the ratio of positive to negative current derivative. To increase the amplitude and, depending on the simulator design, the width of the initial pulse, a copper-ring structure was added to the modified generator.

As an example of the parametric studies done, the geometries shown in Figs. 35 and 36 and their effect on the current, shown in Fig. 37, was studied.
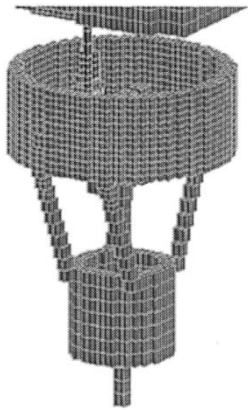
Fig. 36.   Discharge tip with copper ring. The copper-ring structure is connected to the high-voltage potential through a 135-Ω resistor.
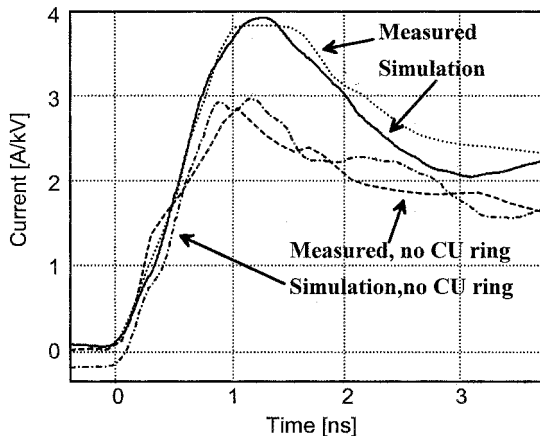

Fig. 37.   Comparison of ESD generators with and without a copper-ring structure.

As shown in Fig. 37, the copper ring increases the initial peak current. It also increases the electrostatic field around the simulator to approximate the electrostatic field of a hand.

B. Ground-Strap Current Compared With Discharge Current at the Tip

The time-domain data presented in Figs. 27 and 23 indicate larger high frequency components in the discharge tip current relative to the current in the ground-strap end. The spectral analysis reveals this in much greater detail: Above 120 and up to 800 MHz, the ground-strap current has at least 10 dB less spectral current density than the current at the discharge point.

VIII. CONCLUSION

A numerical model for the simulation of ESD generators has been proposed and validated. The simulation results are able to predict the current and field waveforms of ESD generators based on the charge voltage and the geometry. The accuracy of the results is sufficient for parametric studies. The model is suitable to calculate the coupling into structures. It allows predicting and investigating the reasons for differences in test results if the ESD generator brand is changed.

ACKNOWLEDGMENT

REFERENCES

[1] "Electromagnetic compatibility (EMC)—Part 4–2: Testing and measurement techniques—Electrostatic discharge immunity test,", EN 61 000-4-2:1995, Amendment 1:1998, Amendment 2: 2001, 2001.

[2] J. Maas and D. J. Pratt, "A study of the repeatability of electrostatic discharge simulators," in *Proc. IEEE Int. Symp. Electromagnetic Compatibility*, 1990, pp. 265–269.

[3] W. Rhoades and J. Maas, "New ANSI ESD standard overcoming the deficiencies of worldwide ESD standards," in *Proc. IEEE Int. Symp. Electromagnetic Compatibility*, vol. 2, 1998, pp. 1078–1082.

[4] D. Pommerenke, "ESD: What has been achieved, what is less well understood?," in *Proc. IEEE Int. Symp. Electromagnetic Compatibility*, Zurich, Switzerland, Feb. 1999, pp. 77–82.

[5] S. Frei and D. Pommerenke, "Fields on the horizontal coupling plane excited by direct ESD and discharges to the vertical coupling plane," *J. Electrostat.*, pp. 177–190, 1998.

[6] L. M. MacLeod and K. G. Balmain, "Compact traveling-wave physical simulator for human ESD," *IEEE Trans Electromagn. Compat.*, vol. 39, pp. 89–99, May 1997.

[7] D. Pommerenke and M. Aidam, "ESD: Waveform calculation, field and current of human and simulator ESD," *J. Electrostat.*, vol. 38, pp. 33–51, Nov. 1996.

[8] R. Jobava, D. Pommerenke, D. Karkashadze, P. Shubitidze, R. Zaridze, S. Frei, and M. Aidam, "Computer simulation of ESD from voluminous objects compared to transient fields of humans," *IEEE Trans Electromagn. Compat.*, vol. 42, pp. 54–65, Feb. 2000.

[9] R. Giannetti and B. Tellini, "Equivalent network modeling to simulate electrical discharges," *IEEE Trans. Magn.*, vol. 36, July 2000.

[10] P. Leuchtmann and J. Sroka, "Transient field simulation of electrostatic discharge (ESD) in the calibration setup (ace. IEC 61 000-4-2)," in *Proc. IEEE Int. Symp. Electromagnetic Compatibility*, vol. 1, 2000, pp. 443–448.

[11] ——, "Enhanced field simulations and measurements of the ESD calibration setup," in *Proc. IEEE Int. Symp. Electromagnetic Compatibility*, vol. 2, 2001, pp. 1273–1278.

[12] O. Fujiwara and K. Kawaguchi, "FDTD analysis of electromagnetic fields due to spark between charged metals with ferrite material attachment," *Proc. IEEE Int. Symp. Electromagnetic Compatibility*, pp. 134–137, 1999.

[13] M. Angeli and E. Cardelli, "Numerical modeling of electromagnetic fields generated by electrostatic discharges," *IEEE Trans. Magn.*, pt. 2, vol. 33, pp. 2199–2202, Mar. 1997.

[14] F. Maradei and M. Raugi, "Analysis of upsets and failures due to ESD by the FDTD-INBC's method," in *Proc. IEEE Industry Applications Conf.*, vol. 1, 2000, pp. 623–630.

[15] R. L. Gardner, L. Baker, C. E. Baum, and D. J. Andersh, "Comparison of lightning with public domain HEMP waveforms on the surface of aircraft," in *Proc. 6th Int. Symp. Electromagnetic Compatibility*, Zurich, Switzerland, 1985, pp. 175–180.

[16] J. Sroka, "Insertion loss as transfer coefficient for the calibration of ESD simulators. Is it sufficient to cope with?," in *Proc. IEEE Int. Symp. Electromagnetic Compatibility*, vol. 2, 2001, pp. 838–840.

[17] ——, "Contribution of the target in the measurement uncertainty by calibration of the ESD simulator," in *Proc. 14th Int. Symp. Electromagnetic Compatibility*, Feb. 2001, pp. 189–192.

[18] Zeland Software. Fidelity created by Zeland Software. Zeland Software, Fremont, CA. [Online]. Available: www.zeland.com

[19] O. Fujiwara and M. Nomura, "Approximation of surface-SAR in a realistic head model for microwave exposure using external magnetic nearfield," *IEICE Trans. Commun.*, vol. E78-B, no. 2, pp. 140–144, 1995.
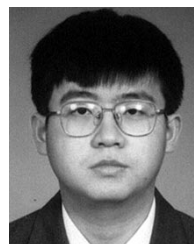
Kai Wang received the B.S. and M.S. degrees in electrical engineering from Tsinghua University, Beijing, China, in 1998 and 2000, respectively. He is currently working toward the Ph.D. degree at the University of Missouri, Rolla.

Since 2001, he has been with the Electromagnetic Compatibility Laboratory, University of Missouri, under the direction of Dr. Pommerenke. His research interests include numerical and experiential study of electrostatic discharge and signal integrity problems, as well as advanced RF measurement.

David Pommerenke was born April 11, 1962, in Ann Arbor, MI. He received the diploma in electrical engineering and the Ph.D. degree on "transient fields of electrostatic discharge (ESD)," from the Technical University Berlin, Berlin, Germany, in 1989, and 1995, respectively.

He was a Research and Teaching Assistant in the areas of electromagnictic compatibility and high voltage at the Technical University Berlin. He joined Hewlett-Packard, Roseville, CA, in 1996. He became an Associate Professor in the Electromagnetic Compatibility Group, University of Missouri-Rolla, Rolla, in 2001. His areas of interest are electromagnetic compatibility, ESD, numerical calculation, high-voltage partial discharge detection systems, and electronics and design of test and measurement equipment. Relevant to the ESD work, he is a member of IEC TC77b WG-9, the working group that sets the IEC 61 000–4–2 ESD test standard.

Ramachandran Chundru was born in India in 1977. He received the B.S.E.E. degree from the University of Madras, Chennai, India in 2000, and the M.S.Comp.E. degree from the University of Missouri, Rolla, in 2001, where he is currently working toward the M.S.E.E. degree.

Since 2001, he has been studying and working in the Electromagnetic Compatibility Laboratory at the University of Missouri. His research interests include electrostatic discharge (ESD), electromagnetic compatibility, signal integrity, shielding problems, susceptibility problems, ESD testing, as well as advanced RF measurements.

Tom Van Doren (S'60–M'69–SM'96–F'02) is a Professor of electrical and computer engineering at the University of Missouri, Rolla. For the past 25 years, his teaching and research has focused on electromagnetic compatibility.

James L. Drewniak (S'85–M'90–SM'01) received the B.S. (highest honors), M.S., and Ph.D. degrees in electrical engineering, all from the University of Illinois, Urbana-Champaign, in 1985, 1987, and 1991, respectively.

In 1991, he joined the Electrical Engineering Department at the University of Missouri, Rolla, where he is a Professor and is affiliated with the Electromagnetic Compatibility Laboratory. His research interests include the the development and application of numerical methods for investigating electromagnetic compatibility problems, packaging effects, and antenna analysis, as well as experimental studies in electromagnetic compatibility and antennas.

Prof. Drewniak is an Associate Editor of the IEEE TRANSACTIONS ON ELECTROMAGNETIC COMPATIBILITY.

Ashwin Shashindranath is a sophomore pursuing the Bachelor's degree in electrical engineering from the University of Missouri, Rolla.

He is a Research Assistant in the Electromagnetic Compatibility Laboratory, University of Missouri. His research areas include working on commercial numerical modeling softwares like Fidelity.